DOI: 10.1002/ejic.201100367

Syntheses, Structure, Physical Properties, and Electronic Structures of $DyCu_xAl_{12-x}$ ($4.0 \leq x \leq 6.0$)

Hua Lin,[a,b] Wei-Zhao Cai,[a,b] Yong-Fang Shi,[a,b] and Ling Chen*[a]

Dedicated to Professor John D. Corbett on the occasion of his 85th birthday

Keywords: Solid state reactions / High temperature reactions / Intermetallic phases / Conducting materials / Rare earths / Dysprosium / Copper / Aluminium / Electronic structure / Magnetic properties

The title phases are synthesized from an elemental mixture by high temperature solid-state reactions and the single-crystal structure refinement of $DyCu_{5.51(4)}Al_{6.49(4)}$ reveals its $ThMn_{12}$-type structure. The structure can be viewed as a 3D condensed network of Dy-centered, 20 vertex $[Al_4Cu_8M_8]$ polyhedra, in which Cu/Al disorder has been observed on the *M* site (8*j*). A homogeneous range of $DyCu_xAl_{12-x}$ ($4.0 \leq x \leq 6.0$) has been observed. The metallic electrical conductivities of $DyCu_xAl_{12-x}$ decrease as x increases following the decreasing trend of the densities of states at the Fermi level based on tight-bonding linear muffin-tin orbital (TB-LMTO) calculations.

Introduction

Ternary rare earth/Cu/Al systems represent a class of polar intermetallic compounds that provide numerous opportunities to study relationships between the crystal structure, chemical bonding, chemical composition, and physical properties.[1–6] Previous studies based on powder XRD data have indicated that $DyCu_4Al_8$ adopts a $ThMn_{12}$-type structure (space group *I*4/*mmm*, Pearson symbol *tI*26), in which the Dy and Cu atoms occupy the 2*a* and 8*f* positions and Al the 8*i* and 8*j* positions.[7] Another powder XRD study has concluded the same distribution of Dy, Cu, and Al on the 2*a*, 8*f*, and 8*i* sites, respectively, with disorder over the 8*j* sites with occupancies of 50% Cu and 50% Al, which generates a composition of $DyCu_6Al_6$.[5] These studies have revealed that the occupancy of Cu on the 8*j* sites varies between 50% and zero. It will be interesting to see if a phase width for $DyCu_xAl_{12-x}$ exists. In addition, to the phase width of $DyFe_xAl_{12-x}$ ($4.0 \leq x \leq 4.7$) in the Dy/*M*/Al (*M* = Cr, Mn, Co, Ni),[5,8,9] the homogeneity range of related structures, such as AM_xB_{13-x} (*A* = Ba, Sr, La, Eu; *M* = Cu, Ag; *B* = Al, Ga, In; $5 \leq x \leq 6.5$) of $NaZn_{13}$-type has been described.[10–13]

We report our continued studies on the $DyCu_xAl_{12-x}$ phase and our findings of an intermediate Cu occupancy on the 8*j* sites by single-crystal diffraction data, the phase width, magnetic properties, and electrical conductivity as well as the TB-LMTO electronic band structure calculations.

[a] Key Laboratory of Optoelectronic Materials Chemistry and Physics, Fujian Institute of Research on the Structure of Matter, Chinese Academy of Sciences,
Fuzhou, Fujian 350002, People's Republic of China
Fax: +86-591-83704947
E-mail: chenl@fjirsm.ac.cn
[b] Graduate School of the Chinese Academy of Sciences, Beijing 100039, People's Republic of China

Results and Discussion

Structure

The structure of $DyCu_{5.51(4)}Al_{6.49(4)}$ is a $ThMn_{12}$-type structure (space group *I*4/*mmm*, *Z* = 2, Pearson symbol *tI*26). The single crystal data refinement indicates that the Dy, Cu1, and Al1 atoms occupy the 2*a*, 8*f*, and 8*i* sites, respectively. The 8*j* sites (nominated as *M*) are shared by 36.8(4)% Cu2 and 63.2(4)% Al2 atoms (see Tables 1 and 2). Similar disorder on the 8*j* sites with half and half Cu/Al occupancy has been found in $DyCu_6Al_6$,[5] although the composition of $DyCu_4Al_8$ results from the full occupation of Al in the 8*j* sites.[7] As shown in Figure 1, the structure can be viewed as a 3D condensed network of Dy-centered, 20 vertex $[Al_4Cu_8M_8]$ polyhedra. The 20 vertices of each polyhedron consist of 4 Al atoms at the 8*i* sites, 8 Cu atoms

Table 1. The cell parameters of $DyCu_xAl_{12-x}$ from powder diffraction data.

Loading ratio	*x*	*a* [Å]	*c* [Å]	*V* [Å^3]
$DyCu_4Al_8$	4.0	8.698(6)	5.127(6)	387.93
$DyCu_{4.5}Al_{7.5}$	4.5	8.693(7)	5.121(6)	387.07
$DyCu_5Al_7$	5.0	8.667(7)	5.104(6)	383.47
$DyCu_{5.5}Al_{6.5}$	5.5	8.656(4)	5.093(3)	381.68
$DyCu_6Al_6$	6.0	8.648(5)	5.048(5)	377.67

at the 8*f* sites, and the remaining are *M* atoms that are randomly distributed Cu and Al atoms (Figure 2, a). Each polyhedron shares its 8*f* Cu vertices with neighboring polyhedra as indicated in Figure 1, and shares the quadrangular *M*4 faces in the *c* direction. (Figure 2, b).

Table 2. Crystal data and structural refinements for $DyCu_{5.51(4)}Al_{6.49(4)}$.

Empirical formula	$DyCu_{5.51(4)}Al_{6.49(4)}$
Formula weight	687.71
Space group	*I*4/*mmm* (No. 139)
a [Å]	8.694(7)
c [Å]	5.116(5)
V [Å^3]	386.8(6)
Z	2
Crystal size [mm]	0.12/0.10/0.09
Temperature [K]	293(2)
ρ_{cal} [g/cm^3]	5.905
Radiation, λ [Å]	Mo-K_α, 0.71073
Index ranges	$-10 \le h \le 11$
	$-11 \le k \le 7$
	$-6 \le l \le 6$
θ range (°)	3.31–27.49
Collected / unique reflections	1469 / 153
R_{int}	0.0625
μ [mm^{-1}]	25.043
R_1 / wR_2 [$I > 2\sigma(I)$][a]	0.0220 / 0.0470
R_1 / wR_2 [all data]	0.0221 / 0.0470
Largest diff. peak / hole [e Å^{-3}]	2.432 / –0.894
Goodness of fit on F_o^2	1.236

[a] $R_1 = \sum||F_o| - |F_c||/\sum|F_o|$ for $F_o^2 > 2\sigma(F_o^2)$; $wR_2 = \sum[w(F_o^2 - F_c^2)]/\sum[w(F_o^2)^2]^{1/2}$, where $w = 1/[\sigma^2F_o^2 + (AP)^2 + BP]$, and $P = (F_o^2 + 2F_c^2)/3$.

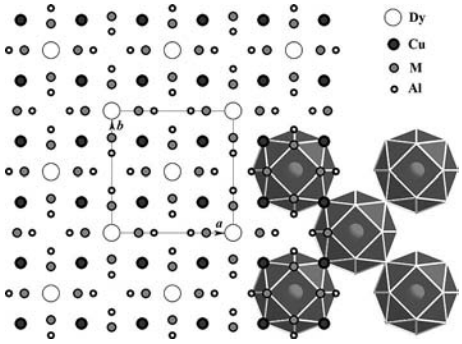

Figure 1. Structure of $DyCu_{5.51(4)}Al_{6.49(4)}$ viewed along the *c* axis. The unit cell, Dy-centered polyhedra, and their connectivity are outlined.

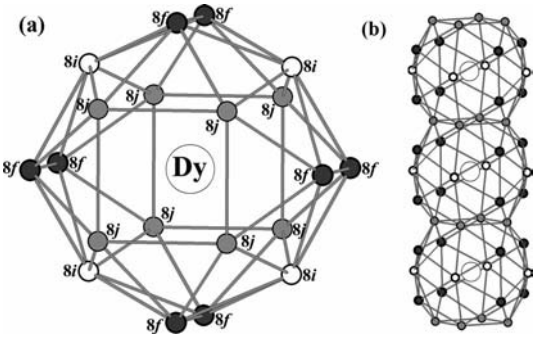

Figure 2. (a) Dy-centered, 20 vertex polyhedron with Wyckoff sites marked. (b) Dy-centered, 20 vertex polyhedra sharing quadrangular *M*4 faces along the *c* direction.

The Cu/Al mixed occupancy is also found in other intermetallics containing Cu and Al.[12,14,15] For instance, $Dy_3Cu_{2.6}Al_{8.4}$ (La_3Al_{11}-type), in which the 4*j*, 8*l*, and another 8*l* site are jointly occupied by Al and Cu atoms with Al/Cu occupancies of 82/18, 95/5, and 48.4/51.6, respectively.[15]

The Dy–*M* distance of 3.197(2) Å is consistent with previously reported values, such as $DyCu_6Al_6$ (Dy–Al/Cu: 3.186 Å),[5] $Dy_3Cu_{2.6}Al_{8.4}$ (3.112–3.265 Å),[15] and $DyCu_4Al$ (2.924 and 3.274 Å).[16]

The Cu–Cu bond length is 2.558(3) Å, which is slightly longer than that of 2.555 Å in *fcc* copper[17] and 2.509 Å in $CaCu_5$,[18] however, falls in the range of those of $DyCu_4Al_8$ (2.569 Å)[7] and $DyCu_6Al_6$ (2.521 Å).[5] The Cu–Al bond of 2.659(2) Å is shorter than the sum of the radii of Cu and Al atoms (2.709 Å),[18] and comparable to those in $CeCu_4Al_8$ (2.570–2.755 Å)[19] and $DyCu_6Al_6$ (2.651 Å).[5] The Al–Al bond length of 2.663(5) Å is shorter than that of 2.864 Å in *fcc* aluminum,[17] but similar to 2.6748–2.6936 Å in $BaAl_4$.[20] The Al–*M* bond lengths range from 2.771(3) to 2.784(3) Å and the Cu–*M* distance is 2.535(2) Å. These data are consistent with those observed in $DyCu_6Al_6$ (Al–*M* 2.744 Å and Cu–*M* 2.512 Å).[5]

Phase Widths of $DyCu_xAl_{12-x}$ ($4.0 \le x \le 6.0$)

As shown in Figure 3, the experimental XRD patterns agree well with those simulated from the single-crystal data, and thus the phase purity of the as synthesized product is confirmed. A series of reactions with different loading ratios, $DyCu_xAl_{12-x}$ (x = 4.0, 4.5, 5.5, 5.0, and 6.0) was carried out with the same heating conditions as described (see Exp. Section). Based on the powder XRD data, pure phase $DyCu_xAl_{12-x}$ was synthesized in the range of $4.0 \le x \le 6.0$, and the corresponding lattice parameters are listed in Table 1. Unknown and impure phases of Cu_4Al_9[21] were observed when $x < 4.0$ or $x > 6.0$. The refined lattice pa-

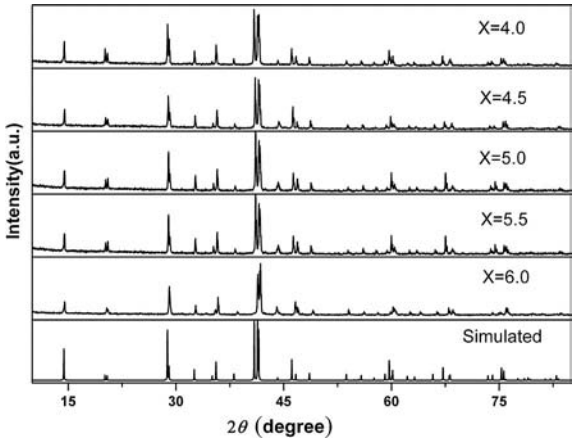

Figure 3. Experimental XRD patterns of $DyCu_xAl_{12-x}$ (x = 4.0, 4.5, 5.0, 5.5, and 6.0) and simulated patterns based on single-crystal data of $DyCu_{5.51(4)}Al_{6.49(4)}$.

rameters gradually decreased as the proportion of Cu increased. This trend is consistent with the shorter Cu–Cu bond length [2.558(3) Å] vs. the Al–Al bond length [2.663(5) Å].

Physical Properties

Magnetic susceptibility measurements for $DyCu_{5.51(4)}Al_{6.49(4)}$ were measured at an applied field of 5000 Oe in the temperature range 2–300 K. As shown in Figure 4, the magnetic susceptibility (χ) vs. temperature (T) shows an antiferromagnetic transition below T_N = 6.5 K, above which the inverse susceptibility (Figure 4, inset) increases linearly with the temperature obeying the Curie–Weiss law, $\chi_M = C/(T - \theta)$, where χ_M is the magnetic susceptibility, C is the Curie constant, and θ is the Weiss constant. According to the equation $\mu_{eff} = (7.997\ \chi_M T)^{1/2}\mu_B$,[22] the calculated effective magnetic moment, $\mu_{eff\ (calcd)}$, is 10.46 μ_B and θ is –12.68 K. The measured μ_{eff} agrees with the calculated $\mu_{eff\ (calcd)} = g[J(J + 1)]^{1/2}\mu_B = 10.63\ \mu_B$ for Dy^{3+} ions, indicating that the magnetic origin mainly arises from the interactions between Dy^{3+} atoms.[23] The minus sign of the θ value indicates antiferromagnetic coupling in this compound. These values are in agreement with those for $DyCu_6Al_6$ (T_N = 3.9 K; μ_{eff} = 10.9 μ_B; θ = –14),[24,25] $DyCu_4Al_8$ (T_N = 17 K; μ_{eff} = 10.6 μ_B; θ = –5),[7] and Dy(Cu, Ga)$_{12}$ (T_N = 6.7 K; μ_{eff} = 10.85 μ_B; θ = –1.16).[6] Since Cu in $DyCu_xAl_{12-x}$ ($4.0 \le x \le 6.0$) is nonmagnetic, the slight composition change should not affect the magnetic behavior of these compounds.

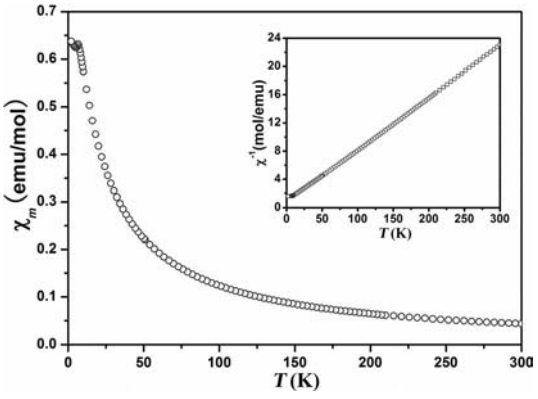

Figure 4. Magnetic susceptibility $\chi(T)$ plot for $DyCu_{5.51(4)}Al_{6.49(4)}$ in a magnetic field of 5000 Oe. Inset is shown the inverse magnetic susceptibility $\chi^{-1}(T)$.

Figure 5 illustrates the temperature-dependent electrical resistivity, ρ (T), of $DyCu_xAl_{12-x}$ (x = 4.0, 5.5, 6.0), which exhibits a metallic type of conductivity in the temperature range 327 to 487 K. This agrees with those observed from single crystals from 0–300 K.[6] The ρ values are 323, 334, and 361 μΩcm at 327 K, for x = 4.0, 5.51, and 6.0, respectively. The value of ρ increases with x, which is related to the decrease of the corresponding densities of states at the E_F as discussed below. These data on the polycrystalline pellets are of the same magnitude as those from single crystals, such as Dy(Cu, Ga)$_{12}$, which has a ρ value of 85 μΩcm at 300 K.[6]

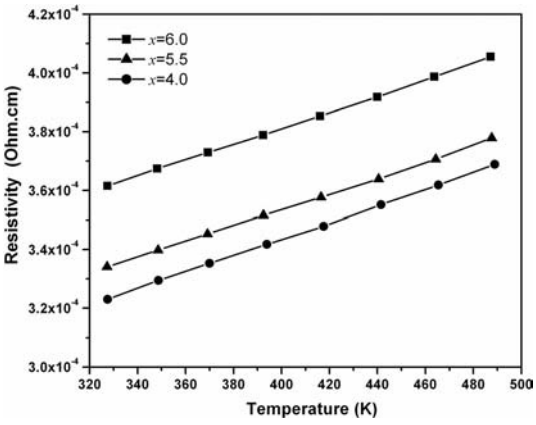

Figure 5. Temperature-dependent electrical resistivity for a cold-pressed polycrystalline pellet of $DyCu_xAl_{12-x}$ x = 4.0, 5.5, 6.0.

Electronic Structures

According to the single-crystal structure refinement results, the disorder of Cu and Al at the M (Wyckoff site 8j) sites generates the composition $DyCu_{5.5}Al_{6.5}$ (x = 5.5). As the radius of Y^{3+} (1.02 Å) is close to that of Dy^{3+} (1.03 Å), Y was used to mimic Dy in order to avoid unconverging calculations considering the localized 4f orbitals of Dy. A model of $Y_2Cu_{11}Al_{13}$ in $P\bar{1}$ symmetry to mimic $DyCu_{5.51}Al_{6.49}$ has been built with three Cu and five Al atoms on the M sites in the most energy favorable pattern as presented in Figure 6. By a similar procedure, two models of $Y_2Cu_8Al_{16}$ and $Y_2Cu_{12}Al_{12}$, representing x = 4 and 6, respectively, were also established. The calculated models were $Y_2Cu_8Al_{16}$, $Y_2Cu_{11}Al_{13}$, and $Y_2Cu_{12}Al_{12}$. The density of states (DOS) and the crystal orbital Hamilton population (COHP) curves for the $Y_2Cu_{11}Al_{13}$ model are displayed in Figures 7 and 8, respectively. The E_F partially

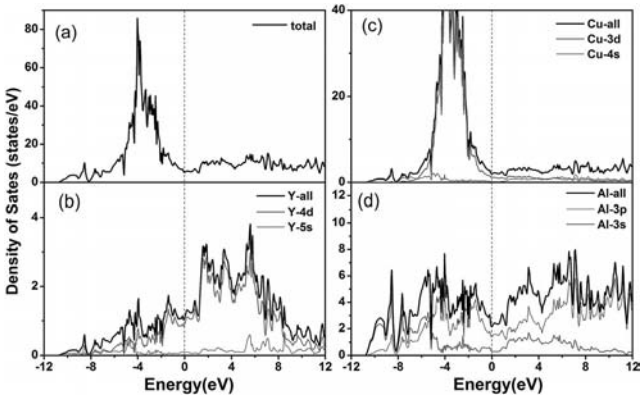

Figure 6. Density of states (DOS) for model $Y_2Cu_{11}Al_{13}$. (a) Total DOS. (b) Partial DOS of Y. (c) Partial density of of Cu 3d and 4s states. (d) Partial density of of Al p and s states. The Fermi level is marked by a dotted line at 0 eV.

crosses the filled bands in the total DOS curve indicating metallic behavior, which is in good agreement with the electrical resistivity measurements. In the region of –5 eV to E_F, the significant mixture of the Cu 3*d* and Al 3*p* states implies a strong covalent bonding interaction between Cu and Al. Most of the Y states (4*d* and 5*s*) are unoccupied and located above the E_F as expected for an electropositive element. A few Y 4*d* states are hybridized with Al 3*p* from –6 to 0 eV, which implies that some bonding behavior between Y and Al. For instance, the Y–Al bonds ranging from 3.016 to 3.197 Å have integrated –COHP values varying from 0.743 to 0.615 eV/cell. As shown in Figure 8 (d), most of the Y–Al and Y–Cu bonding states are populated, whereas the antibonding states remain empty, which is similar to that found in $Ce_4Ni_6Al_{23}$.[26]

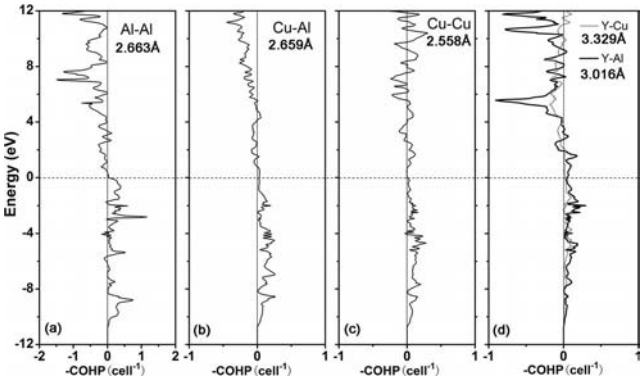

Figure 7. Crystal orbital Hamilton population (COHP) curves for the Al–Al, Cu–Al, Cu–Cu, Y–Cu and Y–Al bonds. The Fermi level is marked by a dotted line at 0 eV.

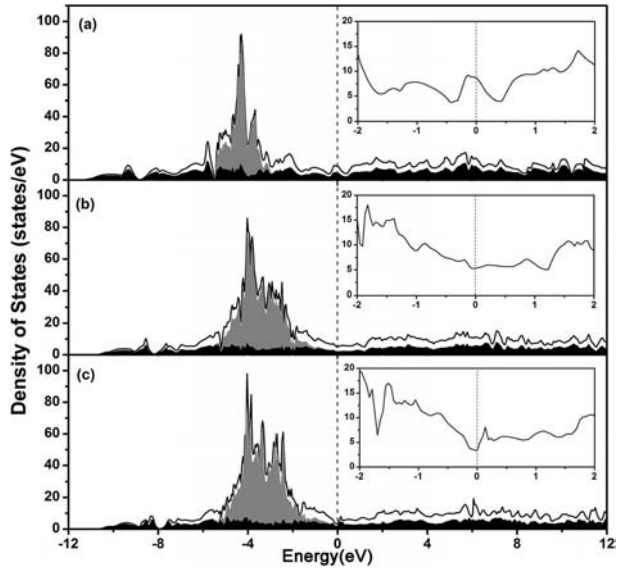

Figure 8. Total DOS for models of (a) $Y_2Cu_8Al_{16}$, (b) $Y_2Cu_{11}Al_{13}$, (c) $Y_2Cu_{12}Al_{12}$; total DOS (solid line), Cu partial DOS (PDOS) (gray region) and Al PDOS (black region). The Fermi level is marked by a dotted line at 0 eV.

The COHP curves in Figure 8 (a) indicate that the Al–Al bonding states are filled, and no antibonding state is occupied below E_F. The Cu–Al interactions in the range of 2.65–2.79 Å have integrated –COHP values from 0.875 to 1.073 eV/cell, which indicate considerable bonding interactions. (Figure 8, b) The Cu–Cu (2.558 Å) bonds show no antibonding interaction below E_F. (Figure 8, c).

The DOS curves for $Y_2Cu_8Al_{16}$, $Y_2Cu_{11}Al_{13}$, and $Y_2Cu_{12}Al_{12}$ representing $DyCu_xAl_{12-x}$, x = 4, 5.5, and 6 are displayed in Figure 9. As the Cu content (x) increases, the Cu 3*d* states display increasing delocalization below E_F. The corresponding values at E_F [N (E_F)] are 8.56, 5.35, and 3.38 states/eV, respectively, which seems follow the same trend as the experimental electrical conductivity of σ ($Y_2Cu_8Al_{16}$) > σ ($Y_2Cu_{11}Al_{13}$) > σ ($Y_2Cu_{12}Al_{12}$).

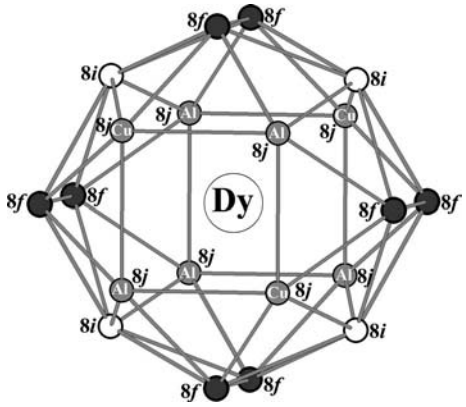

Figure 9. Most energy-favorable arrangement of Cu and Al over 8*j* sites in model $DyCu_{5.51(4)}Al_{6.49(4)}$.

Conclusions

The single-crystal diffraction data reveal that $DyCu_{5.51(4)}Al_{6.49(4)}$ has a $ThMn_{12}$-type structure, which features a 3D condensed network of Dy-centered, 20 vertex [$Al_4Cu_8M_8$] polyhedra, in which Cu/Al disorder occurs at the 8*j* sites. A homogeneous width has been found for $DyCu_xAl_{12-x}$ ($4.0 \leq x \leq 6.0$). With the increase of x, the metallic electrical conductivities of $DyCu_xAl_{12-x}$ (x = 4.0, 5.5, 6.0) decrease, which follows the trend for the decrease of the DOS at E_F.

Experimental Section

Synthesis: Handling of all materials was carried out inside a N_2-filled glove box with oxygen and moisture levels below 0.1 ppm. Dy (99.99% Huhhot Jinrui Rare Earth Co. Ltd), Cu (99.5%, Alfa Aesar), and Al shot (99.99%, ABCR) were used as received. The elements in a stoichiometric ratio of 1:5.51:6.49 (Dy/Cu/Al) were loaded into a graphite crucible, which was enclosed in a fused silica tube and flame-sealed under vacuum (ca. 10^{-3} Pa). The sealed tube was placed into a temperature controlled furnace and the temperature was raised to 1100 °C over 15 h and kept at 1100 °C for 8 h to achieve a proper melt, then cooled to 1000 °C over 1 h and kept at 1000 °C for 40 h, then cooled to 860 °C over 20 h, held at 860 °C for 5 days, slowly cooled to 300 °C at the rate of 4 °C/h, and finally the furnace was switched off. All of the crystals were silver and brittle and were stable when exposed to air for a period of weeks. The chemical composition of the compounds was confirmed with a

field emission scanning electron microscope (FESEM, JSM6700F) equipped with an energy dispersive X-ray spectroscope (EDX, Oxford INCA), which proved that the Dy, Cu, Al were the only elements in the samples.

The phase width was examined with several experiments of different loading ratios, $DyCu_xAl_{12-x}$ ($4.0 \leq x \leq 6.0$) (Table 1). The heating profiles were the same as described above. The powder XRD data were collected with a PANalytical X'Pert Pro diffractometer with Cu-K_α radiation (45 kV × 40 mA) using continuous mode at a rate of 2θ = 4/min. The cell parameters of $DyCu_xAl_{12-x}$ ($4.0 \leq x \leq 6.0$) were obtained by the cell refinement with the aid of JADE 5.0 software package.

Structure Determination: Single-crystal X-ray diffraction data for $DyCu_{5.51(4)}Al_{6.49(4)}$ were collected with a Rigaku Mercury CCD diffractometer equipped with a graphite-monochromated Mo-K_α radiation source (λ = 0.71073 Å) at 293 K. The data were corrected for Lorentz factors, polarization, air absorption, and absorption due to variations in the path length through the detector faceplate. Absorption correction based on a multi-scan technique was also applied.[27] The space group was determined to be *I*4/*mmm* (No. 139) based on systematic absences, *E*-value statistics, and subsequent successful refinements of the crystal structure. All data sets were corrected for Lorentz and polarization factors as well as for absorption by the multi-scan method. The structures were solved by direct methods and refined by full-matrix least-squares fitting on F^2 by SHELX-97.[28] All of the atoms were refined with anisotropic thermal parameters. Initially the 8*j* site was assigned as fully occupied Cu atom, but the refinement resulted unreasonably high *R* values (*R*1 = 8.96%, *wR*2 = 36.16%). Subsequently, the 8*j* site was disordered with Cu and Al with a linear free variable constrain (SUMP), and refinement converged to better *R* values (*R*1 = 2.36%, *wR*2 = 6.82%) with occupancies of Cu2/Al2 = 0.368:0.632, which generated a composition of $DyCu_{5.51(4)}Al_{6.49(4)}$. Crystallographic data and structural refinements are summarized in Table 2. Positional and equivalent isotropic displacement parameters and relevant interatomic distances are listed in Tables 3 and 4, respectively.

Table 3. Atomic positions, site symmetry, and U_{eq} values for $DyCu_{5.51(4)}Al_{6.49(4)}$.

Atom	Wyckoff site	*x*	*y*	*z*	U_{eq} [Å^2][b]
Dy	2*a*	1/2	1/2	1/2	0.0060(3)
Cu1	8*f*	1/4	1/4	1/4	0.0081(3)
M[a]	8*j*	0.2795(2)	1/2	0	0.0104(4)
Al1	8*i*	0.2795(2)	0.99982(9)	0.24994(7)	0.0101(5)

[a] *M* = 36.8(4)% Cu2/63.2(4)% Al2. [b] U_{eq} is defined as one-third of the trace of the orthogonalized U_{ij} tensor.

Table 4. Selected interatomic distances [Å] of $DyCu_{5.51(4)}Al_{6.49(4)}$.[a]

Bond	Length [Å]	Bond	Length [Å]
Dy1–Al1×4	3.016(3)	Cu1–M×4	2.535(2)
Dy1–M×8	3.197(2)	Al1–Al1	2.663(5)
Dy1–Cu1×8	3.3293(2)	Al1–M×2	2.771(3)
Cu1–Cu1×2	2.558(3)	Al1–M×2	2.784(3)
Cu1–Al1×2	2.659(2)		

[a] Distorted *M* sites contain a mixture of 36.8(4)% Cu and 63.2(4)% Al.

Further details on the crystal structure investigation may be obtained from the Fachinformationszentrum Karlsruhe, 76344 Eggenstein-Leopoldshafen, Germany (fax: +49-7247-808-666; e-mail: crysdata@fiz-karlsruhe.de), on quoting the depository number CSD-422807.

Magnetic Susceptibility Measurements: The dc magnetic susceptibility measurements on a powdered $DyCu_{5.51(4)}Al_{6.49(4)}$ sample were performed with a PPMS-9T magnetometer at a field of 5000 Oe cooling from 300 to 2 K. Corrections were made for the susceptibility of the container and the ion core diamagnetism.

Electrical Resistivity Measurements: Electrical resistivity was measured over the temperature range 327.5–487.5 K using a ULVAC ZEM-3 instrument. The powdered samples of $DyCu_xAl_{12-x}$ (x = 4.0, 5.5, 6.0) were cold-pressed into a pellets. $DyCu_4Al_8$ (10.1 × 3.2 × 3.2 mm); $DyCu_{5.51(4)}Al_{6.49(4)}$ (10.1 × 3.3 × 3.1 mm); $DyCu_6Al_6$ (10.1 × 3.14 × 2.1 mm). These pellets were annealed at 623.5 K for 5 h to ensure high density.

Electronic Structure Calculations: According to the single crystal refinement, the *M* (Wyckoff site 8*j*) sites were occupied by a mixture of Cu2/Al2 (%/%) of 36.8:63.2, respectively. A model of $Dy_2Cu_{11}Al_{13}$ in $P\bar{1}$ symmetry to mimic $DyCu_{5.51(4)}Al_{6.49(4)}$ has been built with three Cu and five Al atoms on the *M* sites in the energy most favorable pattern as presented in Figure 6. By a similar procedure, two other models of $DyCu_xAl_{12-x}$ (x = 4, 6) were established. As the radius of Y^{3+} (1.02 Å) is close to that of Dy^{3+} (1.03 Å), the Y atom was used to mimic the Dy atom in order to avoid unconverging calculations considering of the localized 4*f* orbitals of Dy. Thus the three models calculated were $Y_2Cu_8Al_{16}$, $Y_2Cu_{11}Al_{13}$, and $Y_2Cu_{12}Al_{12}$. Electronic band structure calculations were carried out by TB-LMTO.[29–31] Exchange and correlation were treated in the local density approximation.[32] The basis set included the 4*d*, 5*s*, 5*p* orbitals for Y; 3*d*, 4*s*, 4*p* orbitals for Cu, and 3*s*, 3*p*, 3*d* orbitals for Al. The Y 5*p*, Cu 4*p*, and Al 3*d* orbitals were treated with the downfolding technique.[33] The *k*-space integrations were performed by the tetrahedron method[34] using 2 × 4 × 4 *k*-mesh within the Brillouin zone. The E_F = 0 eV was selected as the energy reference.

Acknowledgments

This research was supported by the National Natural Science Foundation of China (NSFC) (projects 90922021, 20733003 and 20973175) and the "Knowledge Innovation Program of the Chinese Academy of Sciences" (KJCX2-YWH20 and CXJJ-11-M71).

[1] U. Häussermann, S. Amerioun, L. Eriksson, C. S. Lee, G. J. Miller, *J. Am. Chem. Soc.* **2002**, *124*, 4371–4383.
[2] J. H. Westbrook, R. L. Fleischer (Eds.), *Intermetallic Compounds: Principle and Practice*, Wiley, New York **1995**.
[3] J. D. Corbett, *Angew. Chem.* **2000**, *112*, 682; *Angew. Chem. Int. Ed.* **2000**, *39*, 670–690.
[4] K. Oe, R. Kobayashi, T. Nishioka, H. Kato, M. Matsumura, K. Kodama, *J. Phys.: Conf., Ser.* **2009**, *150*, 042146.
[5] I. Felner, *J. Less-Common Met.* **1980**, *72*, 241–249.
[6] B. L. Drake, C. Capan, J. Y. Cho, Y. Nambu, K. Kuga, Y. M. Xiong, A. B. Karki, S. Nakatsuji, P. W. Adams, D. P. Young, J. Y. Chan, *J. Phys. Condens. Matter* **2010**, *22*, 066001.
[7] I. Felner, I. Nowik, *J. Phys. Chem. Solids* **1979**, *40*, 1035–1044.
[8] O. Moze, R. M. Ibberson, R. Caciuffo, K. H. J. Buschow, *J. Less-Common Met.* **1990**, *166*, 329–334.
[9] S. Serio, L. C. J. Pereira, M. Godinho, J. C. Waerenborgh, *Intermetallics* **2008**, *16*, 1219–1226.
[10] S. A. Nikitin, I. S. Tereshina, V. N. Verbetsky, A. A. Salamov, E. V. Anosova, *J. Alloys Compd.* **2004**, *367*, 266–269.
[11] M. Wendorff, C. Rohr, *J. Alloys Compd.* **2006**, *421*, 24–34.

[12] K. J. Nordell, G. J. Miller, *Inorg. Chem.* **1999**, *38*, 579–590.
[13] U. Haussermann, C. Svensson, S. Lidin, *J. Am. Chem. Soc.* **1998**, *120*, 3867–3880.
[14] B. M. Stel'makhovych, L. G. Aksel'rud, Y. B. Kuz'ma, *J. Alloys Compd.* **1996**, *234*, 167–170.
[15] B. M. Stel'makhovych, R. V. Gumeniuk, Y. B. Kuz'ma, *J. Alloys Compd.* **2000**, *307*, 218–222.
[16] T. Takeshita, S. K. Malik, W. E. Wallace, *J. Solid State Chem.* **1978**, *23*, 225–229.
[17] J. Donohue, *The Structures of the Elements*, Wiley, New York, **1974**.
[18] G. Bruzzone, *J. Less-Common Met.* **1971**, *25*, 361–366.
[19] O. S. Zarechnyuk, P. I. Kripyakevich, *Kristallografiya* **1962**, *7*, 543–554.
[20] K. R. Andress, E. Alberti, *Z. Metallkd.* **1935**, *27*, 126–125.
[21] A. J. Bradley, *Nature (London)* **1951**, *168*, 661.
[22] C. J. O'Connor, *Prog. Inorg. Chem.* **1982**, *29*, 203–283.
[23] J. H. Van Vleck, *The Theory of Electric and Magnetic Susceptibilities*, Oxford University, Oxford, U.K., **1932**.
[24] I. Felner, M. Seh, M. Rakavy, I. Nowik, *J. Phys. Chem. Solids* **1981**, *42*, 369–377.
[25] I. Felner, M. Seh, I. Nowik, *J. Phys. Chem. Solids* **1981**, *42*, 1091–1095.
[26] D. Gout, E. Benbow, O. Gourdon, G. J. Miller, *J. Solid State Chem.* **2003**, *174*, 471–481.
[27] R. Corp, *CrystalClear*, version 1.3.5, Woodlands, Texas (USA), **1999**.
[28] G. M. Sheldrick, *SHELXL-97: Program for Crystal Structure Solution*, University of Göttingen, Göttingen, Germany, **1997**.
[29] O. K. Andersen, *Phys. Rev. B* **1975**, *12*, 3060–3083.
[30] H. L. Skriver, *The LMTO Method*, Springer, Berlin, Germany, **1984**.
[31] O. Jepsen, O. K. Andersen, *The Stuttgart TB-LMTO Program*, version 4.7, Max-Planck-Institut für Festkörperforschung, Stuttgart, Germany.
[32] U. von Barth, L. Hedin, *J. Phys. C* **1972**, *5*, 1629–1642.
[33] W. R. L. Lambrecht, O. K. Andersen, *Phys. Rev. B* **1986**, *34*, 2439–2449.
[34] P. E. Blöchl, O. Jepsen, O. K. Andersen, *Phys. Rev. B* **1994**, *49*, 16223–16233.

Received: April 6, 2011
Published Online: August 10, 2011

